ELSEVIER

Journal of Power Sources 102 (2001) 1–15

JOURNAL OF POWER SOURCES

www.elsevier.com/locate/jpowsour

Fuel processors for automotive fuel cell systems: a parametric analysis

E. Danial Doss*, R. Kumar, R.K. Ahluwalia, M. Krumpelt

Argonne National Laboratory, Argonne, IL 60439, USA

Received 12 February 2001; accepted 12 March 2001

Abstract

An autothermally-reformed, gasoline-fueled automotive polymer electrolyte fuel cell (PEFC) system has been modeled and analyzed for the fuel processor and total system performance. The purpose of the study is to identify the influence of various operating parameters on the system performance and to investigate related tradeoff scenarios. Results of steady-state analyses at the design rated power level are presented and discussed. The effects of the following parameters are included in the analysis: operating pressure (3 and 1 atm), reforming temperature (1000–1300 K), water-to-fuel and air-to-fuel reactant feed ratios, electrochemical fuel utilization, and thermal integration of the fuel processor and the fuel cell stack subsystems. The analyses are also used to evaluate the impact of those parameters on the concentrations of methane and carbon monoxide in the processed reformate. Both of these gases can be reduced to low levels with adequate water-to-carbon used in the fuel processor. Since these two species represent corresponding amounts of hydrogen that would not be available for electrochemical oxidation in the fuel cell stack, it is important to maintain them at low levels. Subject to the assumptions used in the analyses, particularly that of thermodynamic equilibrium, it was determined that reforming temperatures of 1100 K, a water-to-carbon mole ratio of 1.5–2.5, and the use of fuel cell exhaust energy in the fuel processor subsystem can yield fuel processor efficiencies of 82–84%, and total system efficiencies of 40–42% can be achieved. For the atmospheric pressure system, if the exhaust energy is not used in the fuel processor subsystem, the fuel processor efficiency would drop to 75–82% and the total system efficiency would drop below 40%. At higher reforming temperatures, say 1300 K, the fuel processor efficiency would decrease to 78%, and the total system efficiency would drop below 39%, even with the use of the fuel cell stack exhaust energy.

Keywords: Fuel processing; Fuel cell systems; System modeling; System efficiency

1. Introduction

Fuel cell systems are being developed for powering clean, efficient automobiles of the future. Several prototype fuel cell vehicles have been demonstrated that operate on hydrogen or methanol as the on-board fuel. The polymer electrolyte fuel cell (PEFC) systems being developed for such use require a fuel gas that is either pure hydrogen, or a gas mixture that contains a significant concentration of hydrogen. Thus, the vehicles with methanol as the on-board fuel use a fuel processor, also referred to as a reformer, to convert the methanol to a fuel gas, reformate, that contains hydrogen, carbon dioxide, water vapor, and nitrogen, with trace levels of other species, such as carbon monoxide and unconverted methanol. There is great interest, however, in developing fuel cell vehicles that can operate on the current transportation fuels, primarily gasoline and diesel fuels. Such vehicles would require a fuel processor for gasoline (or diesel) to generate the hydrogen needed by the fuel cell. Several organizations and gasoline (or diesel) to generate the hydrogen needed by the fuel cell. Several organizations and teams are developing gasoline fuel processors for automotive fuel cell systems [1–5]. Using a computer simulation of the fuel processor and the entire fuel cell system, we have analyzed the performance of a generic gasoline autothermal reformer (ATR) for a variety of fuel processor and system designs and values of operating parameters.

In an autothermal fuel processor, the fuel (in this case gasoline, a blend of various hydrocarbons and specific additives), air, and water (steam) are fed in controlled proportions to generate a reformate gas mixture. This reformate must be processed further to convert all the carbon monoxide to carbon dioxide, remove hydrogen sulfide (produced from the organic sulfur typically present in gasoline at 30–300 parts per million, by weight), cool and humidify to the desired fuel cell inlet conditions.

* Corresponding author. Tel.: +1-630-252-5967; fax: +1-630-252-1774.
E-mail address: doss@anl.gov (E. Danial Doss).

0378-7753/01/$ – see front matter
PII: S0378-7753(01)00784-4

The amount and concentration of hydrogen generated from a given amount of gasoline, and the quality of the raw reformate (i.e. CO, CO_2, CH_4 and other hydrocarbons, H_2O, and N_2 contents), are influenced by the reforming conditions. The amount of H_2 produced determines the efficiency of the fuel processor; the greater this amount, the higher is the fuel processor efficiency. The fuel processor efficiency is defined as the ratio of the lower heating value of the total amount of hydrogen in the processed reformate (at the entrance to the fuel cell) to the lower heating value of the gasoline used in the fuel processor. The concentration of H_2 in the reformate influences the performance of the fuel cell stack, with higher hydrogen concentrations yielding better fuel cell performance. The quality of the raw reformate determines the extent of subsequent processing required, primarily for CO and H_2S removal. This subsequent reformate processing has a significant effect on the design, efficiency, volume, weight, and cost of the fuel processing subsystem and, in turn, on the total fuel cell power system.

The primary operating variables in autothermal reforming are the fuel-to-air and fuel-to-water ratios. These two ratios, along with the degree of preheat of the fuel, air, and water (or steam) determine the reaction temperature in the reformer (referred to as the partial-oxidation temperature, T_{POX}, in the present analyses). Other parameters that affect T_{POX} include the degree of fuel conversion, species distribution in the raw reformate, and heat loss from the reformer. Although from this perspective T_{POX} is a dependent variable, in practice T_{POX} is a design parameter, set by the operating temperature of the ATR catalyst. Thus, the primary independent variables must be selected such that the desired T_{POX} is achieved. Different combinations of the fuel-to-air and fuel-to-water ratios may yield the desired T_{POX}; however, with the same T_{POX} but with different feed conditions, the reformate gas composition can be different, in turn yielding different fuel processor and system efficiencies.

The ATR parameters mentioned above are not mutually independent. In addition, many of them must satisfy thermodynamic or practical constraints. For example, certain minimum water-to-fuel and/or air-to-fuel ratios may be needed to prevent carbon formation and deposition during the reforming step. In addition, varying these two ratios would influence the formation of methane, which represents lost hydrogen for the fuel cell stack. As another example, the preheat temperature of the fuel may be limited by the decomposition temperatures of the various species in it, while the preheat temperatures for the steam and air may be limited by materials considerations in their respective heat exchangers. An overall constraint on the various preheat temperatures is the total amount of the thermal energy available from various points in the fuel processing steps and the temperature at which that thermal energy is available. There are also system-level considerations that influence the operation and performance of the fuel processor. These include the system configuration and operating pressure, electrochemical fuel utilization in the fuel cell stack, and the manner of use of the chemical energy in the stack's anode exhaust.

In this paper, we discuss the results of a systematic study of the influence of varying the ATR and system design and operating parameters on the performance of the fuel processor and the total fuel cell system. These analyses offer insight into the various constraints and the research directions that are most likely to lead to efficient fuel processor designs and integration. The analyses have been conducted using GCtool [6], a software package developed at Argonne National Laboratory. GCtool includes component models (of fuel cells, reactors, fluid devices, heat exchangers, etc.), mathematical utilities (non-linear equation solver, ordinary differential equation solver, integrator, constrained non-linear optimizer), and property utilities (thermodynamic data, chemical kinetics, and multiphase equilibria). The model permits variable system configuration, recycle loops, and equality and inequality constraints.

2. The fuel cell system

PEFC systems operating at 3 and 1 atm (absolute) have been modeled and analyzed in previous work [7–9]. The fuel processor subsystem discussed in this paper is a major component of integrated PEFC system. The total PEFC system is defined first, and then the fuel processor subsystem is described next.

Fig. 1 shows a block diagram of the pressurized PEFC system (referred to as the 3 atm system) that was used for the present analyses. The main electric power generator in the system is the fuel cell stack (*pefc*) shown in the upper-right part of Fig. 1. Fuel gas containing H_2 is fed to the fuel side (anode) inlet, and the oxidation air is fed to the air side (cathode) inlet to the stack. The spent fuel gas and air leaving the fuel cell stack are referred to as the anode exhaust and cathode exhaust, respectively. For convenience in describing the fuel cell system configuration shown in Fig. 1, the following paragraphs explain the layout in terms of the flows of air, fuel, process water, exhaust gases, and stack coolant.

Beginning at the top–middle, ambient air is compressed to 3.2 atm (in *cp_air*) and split into two main streams (at *sp_pox*). The smaller airflow to the left is preheated (in *air_htr*) and fed to the ATR partial-oxidation reactor (*pox*). From the larger airflow to the right, a small amount is split off (at *sp_prox*) for injection at the preferential oxidation unit (*prox*) for CO removal. The bulk of the airflow is humidified and cooled by injecting liquid water (at *mx_humc*), and then supplied to the cathode inlet of the fuel cell stack (*pefc*).

The fuel flow circuit begins at the fuel tank (*fuel*) near the bottom-left. From the tank, it is pumped (by *pump_fuel*) to the fuel vaporizer (*fuel_vap*) where it is heated and vaporized by the hot system exhaust gas. It is then fed to the ATR (*pox*) where it is reacted with the preheated air and

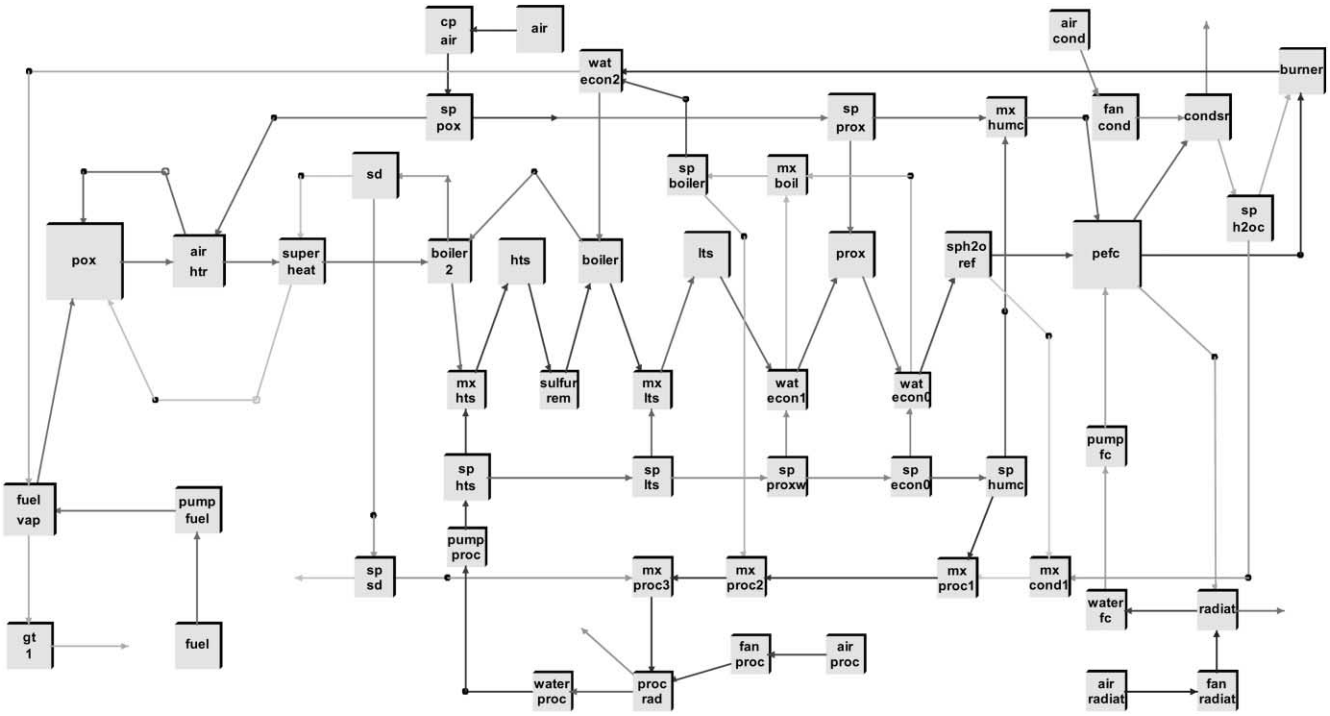

Fig. 1. Configuration of the pressurized gasoline-fueled PEFC system.

superheated steam to yield the raw reformate. The hot reformate is used to preheat the ATR air feed (at *air_htr*), superheat the ATR steam feed (at *super_heat*), and boil the primary process water (in *boiler_2*) for the ATR. It may then be mixed with additional process water (at *mx_hts*) and fed to the high-temperature water–gas shift reactor (*hts*). After removal of H_2S (at *sulfur_rem*) by ZnO or other suitable sorbent, the reformate is further cooled by boiling the process water (*boiler*). The reformate may be then mixed with more water (at *mx_lts*) before entering the low-temperature water–gas shift reactor (*lts*). The fuel gas leaving this reactor is cooled by heating/boiling water in an economizer (*wat_econ1*) and then fed to the preferential oxidation unit (*prox)* for CO removal. The gas exiting *prox* is cooled to the fuel cell stack temperature in another economizer (*wat_econ0*). Any water condensed out is separated (at *sph2o_ref*), and the fuel gas is then fed to the fuel cell stack (*pefc*). Note that the distribution of water addition at *pox*, *mx_hts*, and *mx_lts* may be varied. Indeed, all of the water for fuel processing may be added at the ATR reactor, and the water flows at *mx_hts* and *mx_lts* may be zero, if desired.

The water for fuel processing is taken from a surge tank (*water_proc*) by a water pump (*pump_proc*). Fractions of the process water stream may be split off for the high-temperature shift (at *mx_hts*), the low-temperature shift (at *sp_lts*), the shift reactor exit gas cooler (at *sp_proxw*), the *prox* exit gas cooler (at *sp_econ0*), and the humidifier for the fuel cell air feed (at *sp_humc*). The main process water stream then picks up (at *mx_proc1*) combined water (at *mx_cond1*) from the water separator on fuel cell anode feed (*sph2o_ref*) and the water condensed out of the fuel cell cathode exhaust (*condsr* and *sp_h2oc*). The process water stream then picks up (at *mx_proc2*) any liquid water from the water boilers (*wat_econ0* and *wat_econ1*, combined in *mx_boil*, liquid water separated at *sp_boiler*), and the water from the steam drum (at *mx_proc3*). It then flows to the process water radiator (*proc_rad*) where it is cooled and then returned to the process water tank (*water_proc*). Any excess process water is removed from the return line from the steam drum (*sd*) at (*sp_sd*).

The exhaust gas circuit is best traced from the upper right corner in Fig. 1. The fuel cell cathode exhaust is cooled (in *condsr*) to recover water for the fuel processor (in *sp_h2oc*) and then combined with the anode exhaust in a catalytic burner (*burner*). The hot gas leaving the burner can be used to heat the process water through a heat exchanger (*war_econ2*). The hot gas is then used to vaporize the fuel (in *fuel_vap*) before being expanded in a turbine (*gt_1*) for power recovery. The turbine exhaust is the only exhaust from this fuel cell system.

The last subsystem is the stack coolant circuit which is used to remove the waste heat from the fuel cell stack. Coolant from the tank (*water_fc*) is pumped (*pump_fc*) to the cooling plates in the fuel cell stack. The heated coolant then flows to the main radiator (*radiat*) and then back to the coolant tank (*water_fc*). Although the coolant was assumed to be water in the present analyses, any suitable cooling fluid may be used instead.

The atmospheric pressure system fuel cell system (referred to as the 1 atm system) is shown in Fig. 2. The main differences between 1 and 3 atm system are: (1) the

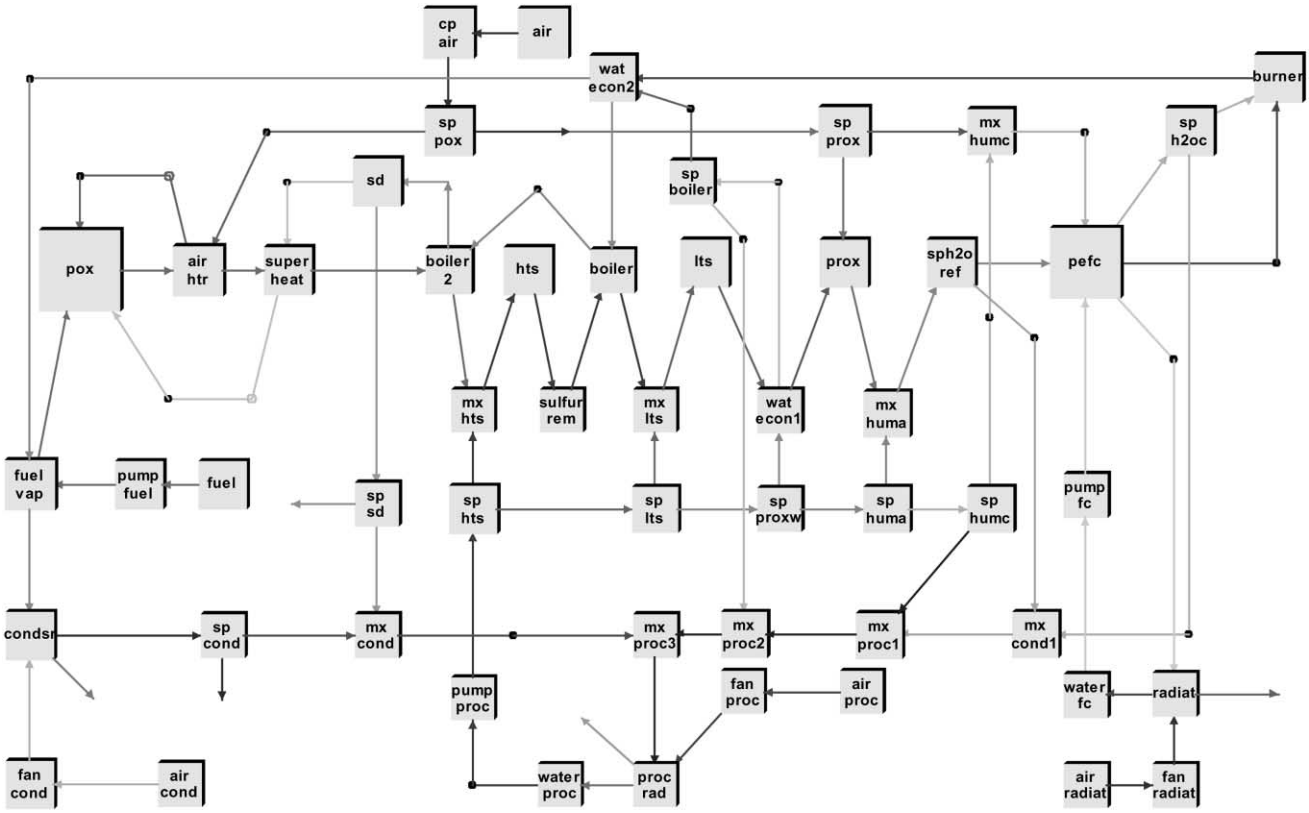

Fig. 2. Configuration of the atmospheric pressure gasoline-fueled PEFC system.

compressor is replaced by a blower (although it is still referred to as *cp_air*, as in Fig. 1) and the expander is eliminated from the system exhaust line; and (2) the condenser to recover the process water is moved from before the fuel cell stack exhaust burner to after the fuel vaporizer in the system exhaust line. The flow lines for the process water subsystem and the exhaust gas after the burner are slightly rearranged to accommodate modified system configuration.

In the pressurized and atmospheric pressure systems described above, the fuel processor subsystem is very similar, except for the additional economizer in the burner exit line for the latter. For the modeling and analysis of the fuel processor subsystem, therefore, both types of systems can be treated in an analogous manner.

3. The fuel processor subsystem

The process of converting gasoline to a fuel gas suitable for feeding to the anode of the fuel cell stack consists of several steps. First, the gasoline is reacted with air and water in the ATR to form a gas mixture of H_2, CO, CO_2, N_2, H_2O, CH_4, and possibly other species, such as H_2S and NH_3. To achieve fuel cell quality gas, all of the CO must be converted to CO_2, and any H_2S, NH_3, or other contaminants must be removed (or reduced to acceptably low levels of a few parts per million or less). The processes for the subsequent processing of the gas mixture produced at the ATR reactor are carried out at successively decreasing temperatures, as discussed below.

The first step, the autothermal reforming reaction, is carried out at the highest temperature in the fuel processing train. Depending on the catalyst used, this reaction may require temperatures of ~1000–1300 K (or higher). At these temperatures, most of the carbon in the fuel is converted to CO or CO_2, with possible formation of relatively small amounts of CH_4 and other hydrocarbons. The reaction conditions must be maintained such that no graphitic or amorphous carbon is formed in this step. For the present analyses, it was assumed that the raw reformate at the exit of the ATR reactor is in thermodynamic equilibrium at T_{POX}. Also, for the cases considered in the analyses, no noticeable carbon was formed under equilibrium calculations. The distribution between CO and CO_2 in this raw reformate is then determined by the reaction temperature and the amount of water/steam in the reactant feed. Lower temperatures and higher amounts of steam favor CO_2 over CO, which is desired. Lower temperatures require an appropriate catalysts, however, and the maximum amount of water is limited by the reaction energetics, since no heat is input to the ATR process as it is in the case of steam reforming.

The bulk of the CO in the raw reformate is converted to CO_2 using the water–gas shift reaction:

$$CO + H_2O \rightarrow CO_2 + H_2 \quad (1)$$

which generates additional H_2 as well. While kinetics would dictate the use of higher temperatures for this reaction, the reaction equilibrium favors the conversion of CO to CO_2 at lower temperatures. Thus, in the fuel processors depicted in Figs. 1 and 2, this water–gas shift reaction is carried out in two stages. The high-temperature shift reactor *hts* is used to convert part of the CO, followed by the low-temperature shift reactor *lts* to provide further reduction in the concentration of CO in the reformate. For the analyses discussed below, the inlet temperature from *hts* was set at 700 K, and the inlet temperature from *lts* was set at 480 K. While GCtool does provide detailed reactor models, for the present analyses it was assumed that the CO and CO_2 are in thermodynamic equilibrium at the respective shift reactor exits. Of course, GCtool ensures that elemental, material, and energy balances are maintained at all times. At these shift reactor temperatures, the CO concentration at the exit from *lts* is typically less than 1% by volume (specific values are discussed below in the results section). This level of CO is still too high for the fuel cell stack which can tolerate only a few parts per million of CO by volume in the fuel gas. The final reduction of CO to these levels is carried out in the preferential oxidizer, *prox*, where the reformate is reacted with a controlled amount of air over a suitable catalyst. The effectiveness factor for this catalyst is assumed to be 50%, i.e. of the oxygen in the injected air, one-half is consumed in oxidizing the CO to CO_2, while the other half oxidizes H_2 in the fuel gas. Thus, the amount of air added at the *prox* is such that the amount of O_2 in it is twice the amount of CO at the inlet to the *prox*. The gas leaving the *prox* is then assumed to have no CO in it.

The fuel processor subsystem shown in Figs. 1 and 2 also includes a fuel gas desulfurizer, *sulfur_rem*. This is treated as a sorbent system with no significant energetics associated with the sulfur removal step. Other components may also be needed, such as a trap for NH_3, which are not included in the analyses. Unless those components have a significant reaction energy, their omission from the analyses would not affect the overall results discussed below.

The other major components of the fuel processing subsystem are the various heat exchangers, boilers, and economizers used for preheating the process streams and heat recovery between the different process steps. This thermal integration is essential for achieving a high efficiency in the fuel processor and in the entire fuel cell power system. For instance, the degree of air preheat and steam superheat for the feeds to the ATR reactor can affect the fuel processing efficiencies significantly. This may be seen in the results for one particular set of analyses shown in Fig. 3, which shows the fuel processor efficiencies as a function of steam superheat temperature for various air preheat temperatures. Fig. 3a shows the results for a pressurized system, while Fig. 3b shows the results for an atmospheric pressure system. In each case, T_{POX} was 1100 K. For both the pressurized and atmospheric systems, the highest fuel processor efficiency is obtained at air and steam preheat temperatures of ~900 K.

At higher values of T_{POX}, similar trends are obtained, i.e. the fuel processor efficiency can, in some cases, be increased by increasing preheat temperatures. The temperatures that can be used in practice may be limited, however, by materials constraints. To avoid temperatures that could require the use of ceramic heat exchangers, it was decided to use air preheat and steam superheat temperatures of 900 K each, for the reactants fed to the ATR reactor for $T_{POX} > 1100$ K, in the systems analyzed below. For $T_{POX} = 1000$ K, however, it was found that the reformate would have inadequate thermal energy to preheat the air to 900 K and raise superheated steam to 900 K over a wide range of water-to-fuel ratios, and also to maintain high fuel processor efficiencies. For this value of $T_{POX} = 1000$ K, it was found that a steam temperature of 750 K and an air preheat temperature of 700 K would give higher fuel processor efficiencies. These temperature values for the preheated air and steam are used in the analyses for the case of $T_{POX} = 1000$ K only. The vaporized gasoline fuel was fed to the ATR reactor at 420 K in all cases. It is worth mentioning at this point that in this set of analyses, all the process water (steam) has been fed into the ATR (*pox*). Therefore, the water-to-fuel and air-to-fuel

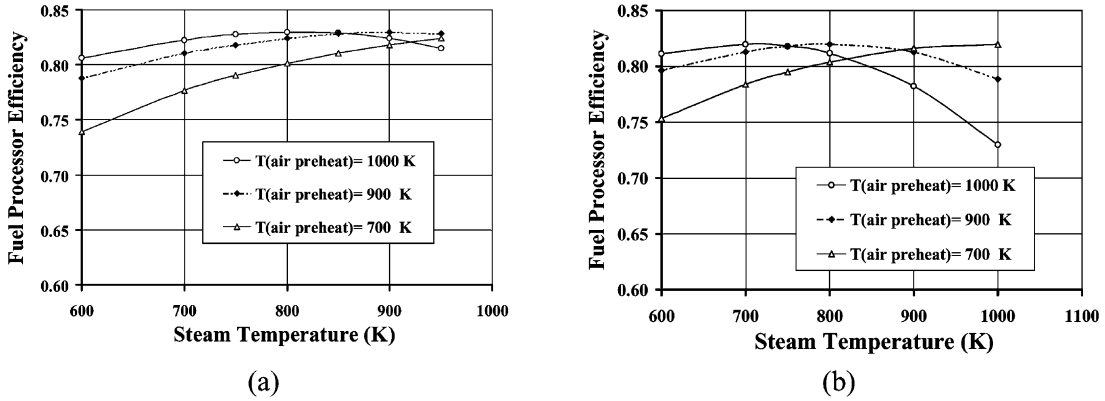

Fig. 3. Effect of steam superheat and air preheat temperatures in the feed to the ATR reactor on the fuel processor efficiency: (a) pressurized 3 atm system; (b) 1 atm system.

ratios were not kept fixed; rather they were computed to meet the temperature constraints imposed on the autothermal and water–gas shift reactors. The influence of these parameters, i.e. the water-to-fuel and air-to-fuel ratios on the fuel processor efficiency is discussed later.

4. Fuel processing parameters

The influence of varying several different fuel processor and fuel cell system design configurations and operating parameters was examined in the present analyses. These include:

1. the temperature of the ATR reactor (T_{POX}, varied from 1000 to 1300 K);
2. water-to-carbon ratio in the ATR reactor feed (from zero to the maximum supported by the energy balance), the water used in the ATR reactor is usually called the primary water;
3. system pressure (1 and 3 atm, nominal);
4. electrochemical fuel utilization in the fuel cell stack (75 and 85%);
5. use or not, of the thermal energy from the fuel cell exhaust gas burner in the fuel processing subsystem.

In general, varying the first two parameters affects other operating parameters, such as the required air-to-fuel ratio (to achieve the desired T_{POX}), CO formation (decreases with decreasing T_{POX} and with increasing water-to-carbon in ATR feed), and CH_4 formation (decreases with increasing T_{POX} and with increasing water-to-carbon in ATR feed). Additionally, varying the last three parameters affects the yield and concentration of hydrogen, and the efficiencies of the fuel processor and the total fuel cell system.

5. Results and discussion

In the following discussion, the results of the analyses are presented as a function of the molar water-to-carbon ratio (or steam-to-carbon ratio, S/C), in the reactants fed to the ATR reactor for various values of the reactor temperature and other parameters. The results for the 3 and 1 atm systems are juxtaposed to enable convenient comparison of the effects of the various parameters discussed above on the two types of systems shown in Figs. 1 and 2, respectively. The nominal fuel cell stack operating temperature was 353 K for the 3 atm system and 343 K for the 1 atm system. The ambient temperature was taken to be 308 K for all cases. At the design 50 kW net electric power from the fuel cell system, the average cell voltage was 0.8 V. For the 3 atm system, the adiabatic efficiencies of the compressor and expander at the design point were taken to be 70 and 80%, respectively. The electrochemical fuel utilization in the fuel cell stack was 85%, except for the cases examining the effect of varying this parameter, for which cases a value of 75% was used.

5.1. Approach

The operation of the fuel processor and the reaction energetics are significantly affected by the water-to-fuel and air-to-fuel ratios in the reactant feed to the ATR reactor. The results discussed below are presented as a function of the primary water used in the ATR reactor, in terms of the water-to-carbon mole ratio (S/C), with different curves for various values of the other parameters. With the specified constraints on the air preheat temperature and the steam superheat temperature discussed earlier, the air-to-fuel ratio that can be used in the fuel processor is determined by T_{POX}, the reaction temperature at the ATR reactor, and by the amount of water that is added to the ATR. The additional water fed to the *mx_hts*, and *mx_lts* is determined by imposing the constraints that the reformate temperatures at the inlet of the corresponding reactors are kept at 700 and 480 K, respectively.

The maximum amount of water that can be fed into the ATR is achieved when no additional water is fed to either *mx_hts*, or *mx_lts*. In this case, the amount of process water added to the ATR is sufficient to quench the reformate in the super heater and the two boilers (*boiler*, *boiler_2*) to the required temperatures of 700 K for the *hts* and 480 K for the *lts*. As the amount of primary water fed to the ATR is reduced, the total thermal energy of the reformate is reduced and its quenching effect will decrease. Therefore, the reformate temperature at the exit of *boiler_2* will be higher than the required temperature of 700 K. In this case, additional water (known as the secondary water) has to be added in *mx_hts* to quench the reformate. As the amount of water fed to the ATR is reduced further, the total thermal energy of the reformate will be reduced even more. At a certain point, the reformate temperature at the exit of the *boiler* will increase above the required temperature of 480 K before *lts*. In this case, additional water will be added to the *mx_lts* to quench the reformate. More discussion will follow, regarding the relation between the total amount of process water (primary and secondary) used in the fuel processor and the amount of primary water used only in the ATR reactor, *pox*.

5.2. Total available water-to-carbon ratio

Figs. 4 and 5 present the variations of the total molar water-to-carbon ratio versus the, primary, *pox* molar water-to-carbon ratio at different *pox* temperatures. The total water-to-carbon mole ratio used in the fuel processor increases with increasing T_{POX} and with increasing S/C in the reactant feed to the ATR reactor. This increase with increasing T_{POX} results from the increased thermal mass of the raw reformate, which permits a greater amount of water to be used. For a given T_{POX}, increasing the amount of water fed at the ATR reactor requires an increase in the amount of air that must also be fed to that reactor, again leading to an increase in the thermal mass of the reformate, with a

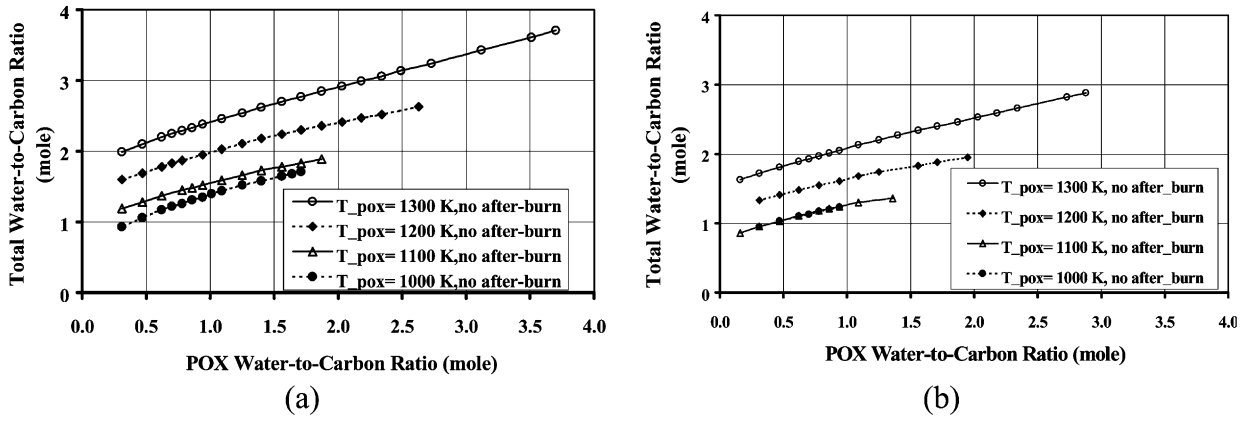

Fig. 4. Total water-to-carbon available for the fuel processor without using the exhaust gas burner heat vs. the water-to-carbon molar ratio in the reactant feed to the ATR reactor: (a) pressurized system; (b) atmospheric pressure system.

concomitant increase in the total amount of water that can be used in the fuel processor.

Fig. 4 shows the results for the 3 and 1 atm systems in which the thermal energy from the fuel cell exhaust gas burner is not used in the fuel processor (designated as ''no after-burn'' in the figure legends). For the 3 atm system, Fig. 4a, the maximum available water-to-carbon mole ratio is 3.7 for $T_{POX} = 1300$ K, decreasing to 1.7 for $T_{POX} = 1000$ K. In the 1 atm system, Fig. 4b, the corresponding maximum water-to-carbon mole ratios are 2.88 at $T_{POX} = 1300$ K, decreasing to 0.94 at $T_{POX} = 1000$ K.

The available water-to-carbon mole ratios increase if the extra thermal energy from the fuel cell exhaust gas burner is used for fuel processing, as shown in Fig. 5 (designated as ''with after-burn'' in the figure legend). For example, for the 3 atm systems with $T_{POX} = 1000$ K, the available water-to-carbon mole ratio increases from 1.7, without after-burn (Fig. 4a) to 2.6 with after-burn (Fig. 5a). For the 1 atm system, the proportionate increase in the water-to-carbon mole ratio is more pronounced. For example, at $T_{POX} = 1000$ K, the S/C molar ratio increases from 0.94, without after-burn (Fig. 4b) to 2.6, with after-burn (Fig. 5b).

These values of the available water-to-carbon mole ratios then define the range over which S/C was varied in the analyses discussed below. In the results shown, the x-axis represents S/C, the water-to-carbon mole ratio in the feed to the ATR reactor. When that value is less than the maximum (derived above), the rest of the water is fed at the high-temperature and/or the low-temperature water–gas shift reactors.

5.3. The fuel equivalence ratio

The reforming conditions at the ATR reactor are defined by the water-to-fuel and the oxygen-to-fuel ratios, along with the inlet temperatures of the fuel (420 K), air, and water/steam. While the water-to-fuel ratio is often given in terms of S/C, the oxygen-to-fuel feed rate is conveniently stated as a fuel equivalence ratio, Φ, for blended fuels. For a given amount of air, Φ is the ratio of the actual amount of fuel reacted to the stoichiometric amount of fuel that would be completely oxidized by the given amount of air. Thus, at a $\Phi < 1$, the gasoline would be completely oxidized to CO_2 and H_2O, with some O_2 also present in the product gas. At $\Phi > 1$, there is not enough oxygen to convert all the carbon

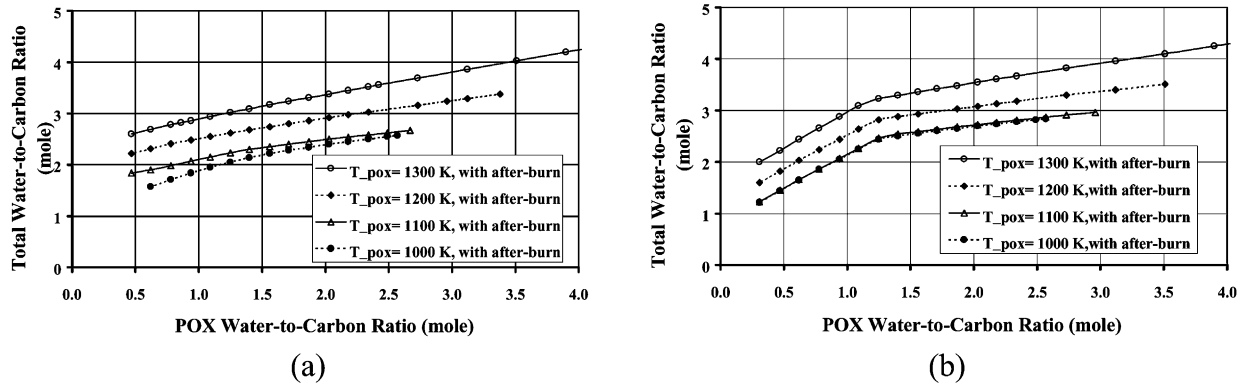

Fig. 5. Total water-to-carbon available for the fuel processor with use of the exhaust gas burner heat in the fuel processing subsystem: (a) pressurized system; (b) atmospheric pressure system.

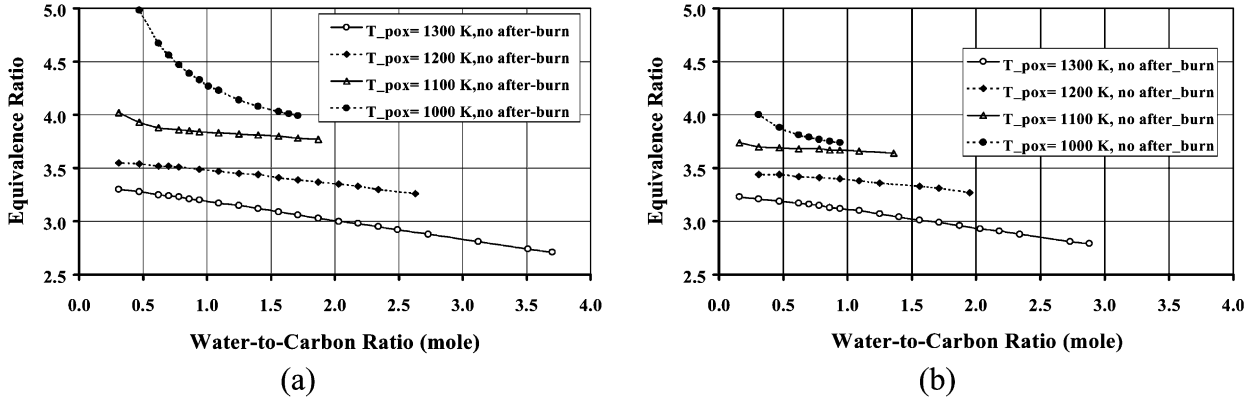

Fig. 6. The fuel equivalence ratio for reforming temperatures of 1000–1300 K: (a) for the 3 atm system; (b) 1 atm system without the use of the fuel cell stack exhaust burner heat in the fuel processor.

in the fuel to carbon dioxide and all the hydrogen in the fuel to water. Under these conditions, the product gas would contain H_2 and/or CO, along with H_2O and CO_2. As Φ increases above 1, the amounts of H_2 and CO also increase (assuming the same percentage conversion of the fuel). The actual product gas composition would be affected by the reaction conditions, such as the reactant feed composition, reaction temperature and pressure, catalyst, etc.

Fig. 6 shows the fuel equivalence ratios for the 3 and 1 atm systems operated with varying values of S/C fed to the ATR reactor. The curves for the different values T_{POX} show what Φ would be needed if no heat from the fuel cell stack exhaust burner is used in the fuel processor. As mentioned above, it is desirable to operate with as high a value of Φ as possible for maximum generation of H_2 and CO (the latter would be subsequently converted to CO_2 and additional H_2 in the water–gas shift reactors). The results in Fig. 6 show that lower reforming temperatures lead to higher values of Φ. For the lower values of T_{POX}, however, the maximum S/C that can be used (subject to the air preheat and the steam superheat constraints discussed above) is limited to relatively low values. At a given T_{POX}, Φ decreases with increasing S/C. For a given reforming temperature and S/C, the Φ is slightly lower for the 1 atm system than for the 3 atm system.

Using the fuel cell stack exhaust burner heat for fuel processing does not affect the Φ significantly for a given T_{POX} and S/C ratio, as shown in Fig. 7. However, the additional energy input does increase the maximum value of S/C for the 3 atm system and more significantly for the 1 atm system. While this would not increase the yield of H_2 by itself, the higher S/C may be helpful in the operation of the reformer, e.g. by suppressing the formation and deposition of carbon (soot).

5.4. Carbon monoxide in the low-temperature water–gas shift reactor exit gas

The high-temperature reforming reaction at the partial-oxidation reformer, *pox*, generates substantial amounts of carbon monoxide, which is converted to carbon dioxide and additional hydrogen in the water–gas shift reactors, *hts* and *lts*. However, even after the shift processing, high levels of CO can be present in the fuel gas, depending on the amount

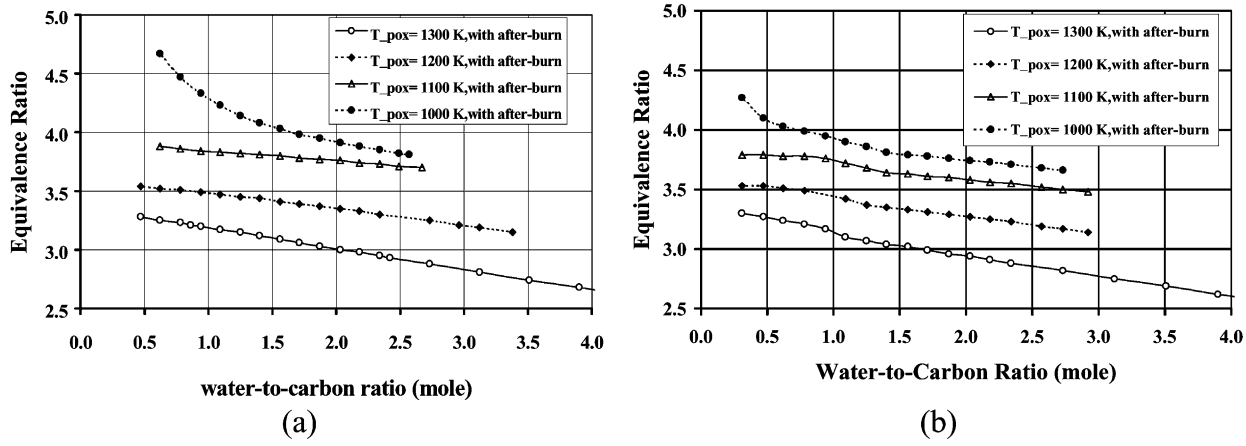

Fig. 7. Effect of using the fuel cell stack exhaust burner heat on the fuel equivalence ratios: (a) for the 3 atm system; (b) 1 atm system.

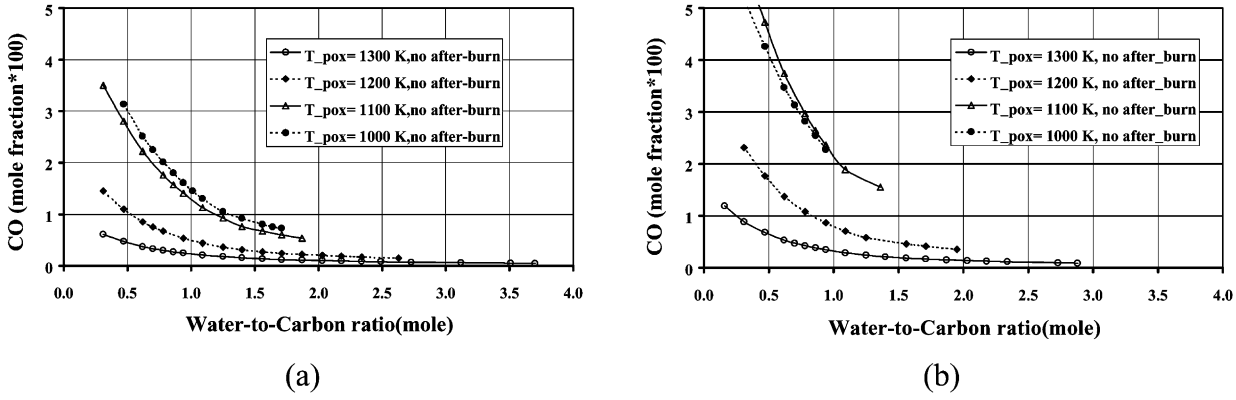

Fig. 8. CO concentration (dry basis) at the exit of the low-temperature shift reactor without use of the burner heat in the fuel processor: (a) for the 3 atm system; (b) 1 atm system.

of S/C fed into *pox* and on the operating temperature of the ATR, T_{POX}. This remaining CO must be almost completely removed in the catalytic preferential oxidizer, *prox*, where it is reacted with 100% excess oxygen. Since this process also consumes an equivalent amount of H_2, it is desirable to reduce the CO concentration by the shift process as much as possible, before it reaches the *prox*. Increasing S/C increases the total amount of water used in the fuel processor, with a resultant decrease in the concentration of CO, as implied by Eq. (1). This effect is evident in the results shown in Fig. 8 for the cases without the use of burner heat and in Fig. 9 for the cases with the use of burner heat in the fuel processor.

5.5. Methane concentration in the reformate

Any methane formed during the autothermal reforming step represents a corresponding decrease in the amount of hydrogen generated by the fuel processor, and a corresponding decrease in the amount of electrical energy generated in the fuel cell stack. This is because the CH_4 does not undergo any reaction in the rest of the fuel processor, and it is not electrochemically oxidized in the fuel cell stack. Its chemical energy is converted to heat at the fuel cell stack exhaust burner, however. Therefore, this CH_4 may or may not result in an efficiency penalty for the fuel processor or the total fuel cell system, depending on how effectively the burner heat can be used in the system.

The concentration of CH_4 in the processed reformate, after *lts*, is greatly affected by the value of T_{POX}, as shown in Figs. 10 and 11, for the cases without and with the use of burner heat in the fuel processor. At high T_{POX} (1100 K or higher) and/or high S/C (>1), the methane slip is less than 0.1%. Only at $T_{POX} = 1000$ K is the significant formation of CH_4 thermodynamically favored.

5.6. Hydrogen concentration in the processed reformate

The concentration of H_2 in the fuel gas supplied to the fuel cell stack affects the performance of the fuel cell, while the amount of total hydrogen obtained from a given amount of gasoline affects the energy conversion efficiency of the fuel cell system. To obtain high performance in the fuel cell, it is desirable to achieve as high a H_2 concentration in the processed reformate as possible.

The discussion presented earlier indicates that there are three identifiable variables that can influence the amount of

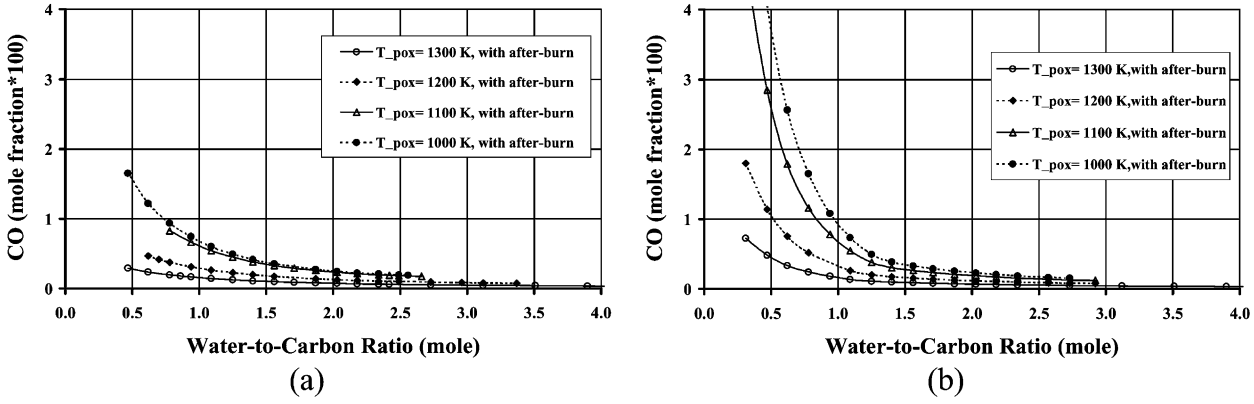

Fig. 9. Effect of using the burner heat on the CO concentration (dry basis) at the exit of the low-temperature shift reactor: (a) for the 3 atm system; (b) 1 atm system.

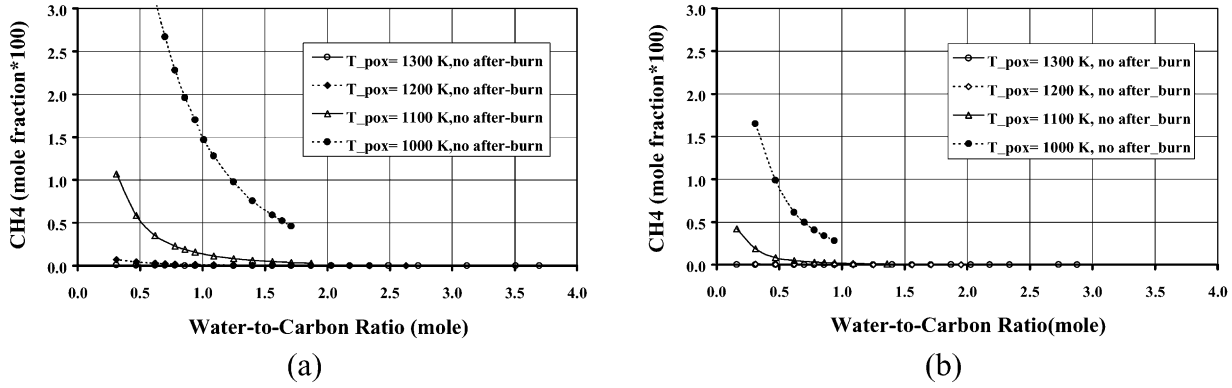

Fig. 10. Concentration of methane (dry basis) in the processed reformate without the use of the burner heat: (a) in the 3 atm system; (b) 1 atm system.

the total hydrogen in the reformate going to the fuel cell stack. These parameters are the fuel-to-air equivalence ratio (*f*), the concentration of CO in the reformate after the low-temperature gas shift, *lts*, and the amount of methane, CH_4, referred to as the methane slip, formed in the autothermal reactor, *pox*.

According to Figs. 6 and 7, lower S/C ratios and/or lower T_{POX}-values, lead to higher values of fuel-to-air equivalence ratio (*f*). Increasing the value of *f* (higher than 1) leads to an increase in the amounts of H_2 formed in the ATR, *pox*. However, according to the results presented in Figs. 8 and 9, the concentration of CO in the reformate after *lts* increases with lower S/C ratios, and with lower T_{POX}-values. In the preferential oxidizer, *prox*, as additional oxygen (air) is injected to react with CO to form CO_2, it also reacts with H_2 and form H_2O. This process leads to a reduction in the total amount of H_2 going to the fuel cell stack. Also, according to Figs. 10 and 11, as the S/C ratio decreases and as T_{POX} decreases, the amount of methane formed in *pox* increases. This increase in the amount of methane formed, leads to a corresponding decrease in the amount of H_2 formed in the fuel processor. Therefore, as S/C ratio decreases and/or T_{POX} decreases, the increase of H_2 formation at higher values of f will eventually be offset by the effects of increased methane formation in *pox* and CO in the reformate after *lts*, as shown in Figs. 12 and 13.

Fig. 12 presents the results for the cases where no heat from the burner is used in the fuel processor. The results with the use of burner heat are shown in Fig. 13. On a dry basis, the H_2 concentration increases with S/C to a maximum at S/C of ~1–2 and then decreases with further increases in S/C. Furthermore, the lower the reforming temperature, the higher is the possible concentration of hydrogen in the processed reformate, for S/C $\geq$ 1.

The use of the burner heat in the fuel processor increases the maximum concentration of H_2 by enabling the use of higher values of S/C at lower values of T_{POX}, (Fig. 13). The highest concentrations of ~46% are obtained at reforming temperatures of 1000–1100 K with the use of burner heat in the fuel processor. Furthermore, the H_2 concentration is relatively insensitive to the S/C-value over a wider range at the lower T_{POX} than it is for higher values, as for T_{POX} of 1300 K, which yields hydrogen concentrations of 41% or less at S/C $\geq$ 1.5.

5.7. Fuel processor efficiency

In addition to the product gas composition, the analyses examined the effect of T_{POX} and S/C on the efficiencies of

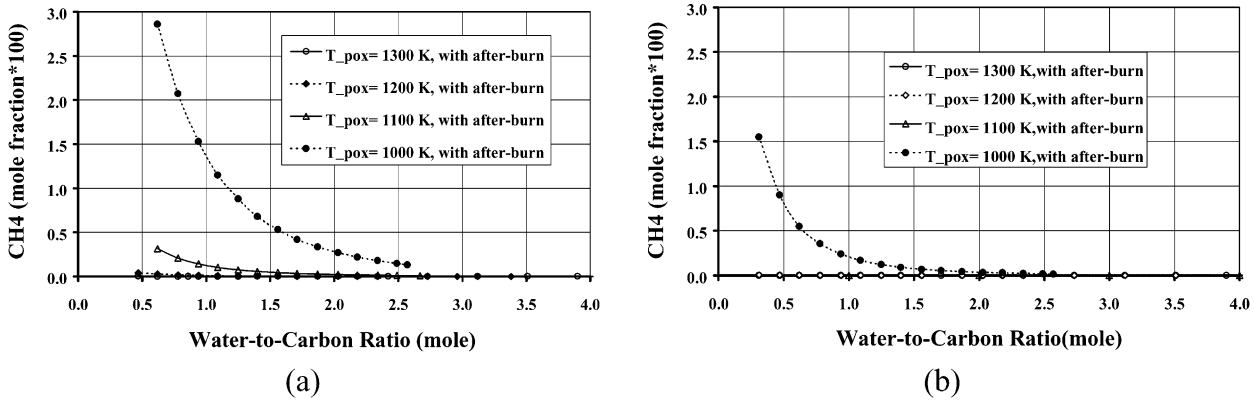

Fig. 11. Effect of using the burner heat on the concentration of methane (dry basis) in the processed reformate: (a) in the 3 atm system; (b) 1 atm system.

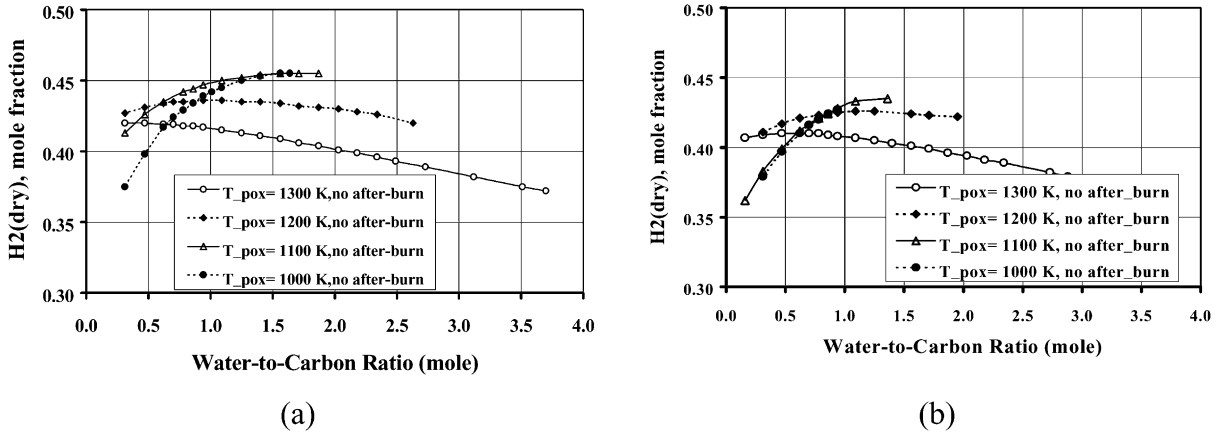

Fig. 12. Hydrogen concentration (dry basis) in the processed reformate without using burner heat in the fuel processor: (a) 3 atm system; (b) 1 atm system.

the gasoline fuel processor (η_{FP}) and of the total system (η_{SYS}). The fuel processor efficiency is defined as the ratio of the lower heating value of the total amount of hydrogen in the processed reformate (fuel gas at the exit of *prox*) to the lower heating value of the gasoline fed to the fuel processor. Therefore, one expects that the trend for the variation of the fuel processor efficiency to follow closely the trend for the variation of the total amount of hydrogen in the processed reformate shown in Figs. 12 and 13.

The fuel processor efficiencies for the cases without the use of the burner heat are shown in Fig. 14. Although there are only small differences between 3 and 1 atm system for $T_{POX} = 1300$ K, at lower reforming temperatures the η_{FP} in the pressurized system is significantly higher than that in the atmospheric pressure system. This difference increases as T_{POX} decreases. Fuel processor efficiencies greater than 80% can be achieved in the 3 atm system. The 1 atm system offers η_{FP} of ~78% or less. Furthermore, in the 3 atm system, η_{FP} increases with decreasing *pox* temperature, except for lower S/C ratios. As discussed before, at lower reforming temperatures, more CH_4 is formed (see Figs. 10 and 11), reducing the amount of H_2 in the processed reformate and, consequently, reducing the efficiency of the fuel processor.

With the use of the burner heat, η_{FP} can be raised by several percentage points as shown in Fig. 15, especially for the atmospheric system. Fuel processor efficiencies of 80–85% are achievable at all reforming temperatures except for 1300 K. For the 3 atm system, η_{FP} is the highest for the reforming temperature of 1100 K over a wide range of S/C ratios. For the 1 atm system, η_{FP} is the highest for reforming temperatures in the range of 1000–1100 K over a wide range of S/C ratios. For lower S/C ratios, η_{FP} still drops rapidly because of methane formation, particularly for the 1 atm case and for reforming temperatures <1200 K.

Another parameter that affects the fuel processor efficiency, η_{FP}, is the electrochemical fuel utilization in the fuel cell stack (U_f). As U_f is varied, the amount of heat available from the fuel cell stack exhaust burner changes, with resultant changes in η_{FP}. Examples of this effect are shown in Fig. 16 for the cases where the burner heat is used in the fuel processor (for the cases where the burner heat is not used for fuel processing, obviously there will be no effect of changes in U_f on η_{FP}). For both the pressurized and atmospheric systems, the fuel processor gains none to a very small advantage in efficiency as U_f is reduced from 85 to 75% (Fig. 16a).

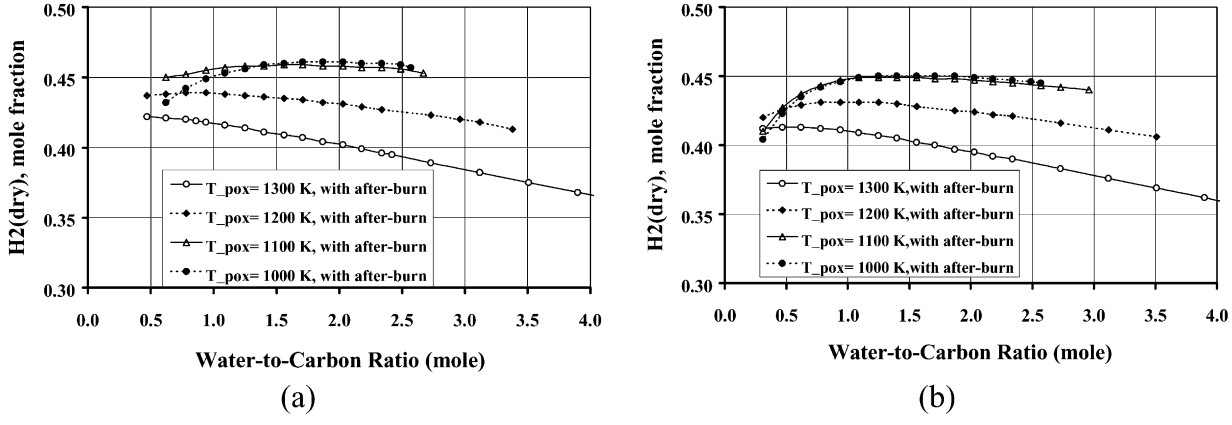

Fig. 13. Effect of using burner heat on the hydrogen concentration (dry basis) in the processed reformate: (a) for the 3 atm system; (b) 1 atm system.

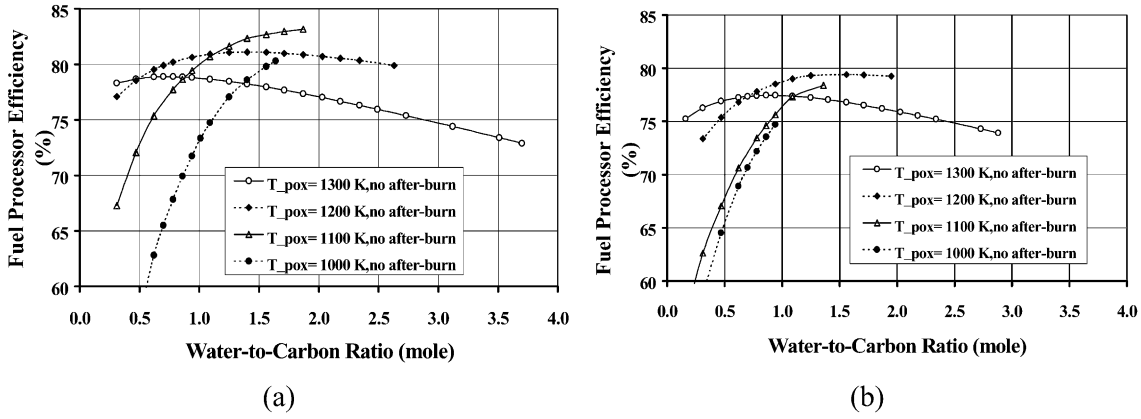

Fig. 14. Fuel processor efficiencies without the use of burner heat: (a) in the 3 atm system; (b) 1 atm system.

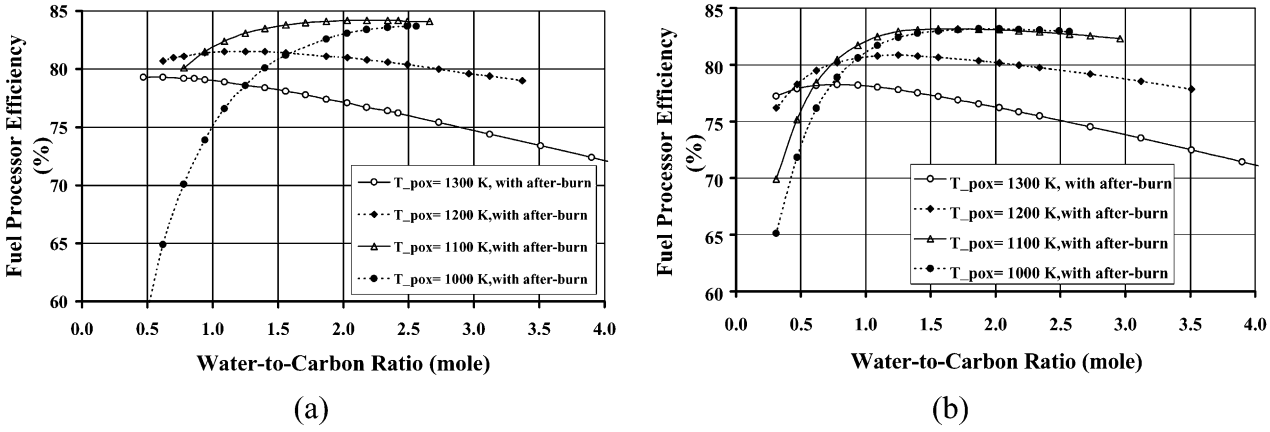

Fig. 15. Increase in fuel processor efficiencies with the use of the burner heat: (a) for the 3 atm system; (b) 1 atm system.

5.8. Total fuel cell system efficiency

More important than the fuel processor efficiency, η_{FP}, however, is the total system efficiency, η_{SYS}. The system efficiency is defined as the ratio of the net power generated by the system to the lower heating value of the fuel (gasoline) fed to the fuel processor. The total power generated in the system includes the power produced by the fuel cell stack (which is directly related to the total amount of hydrogen in the reformate) and the power generated in the gas turbine

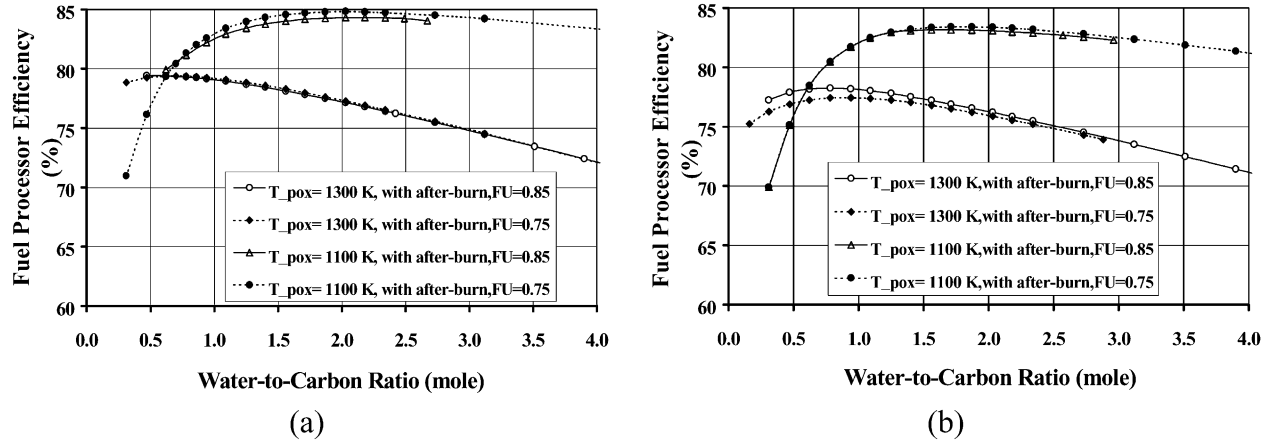

Fig. 16. Effect of electrochemical fuel utilization on the efficiency of the fuel processor for two different reforming temperatures: (a) in the 3 atm system; (b) 1 atm system.

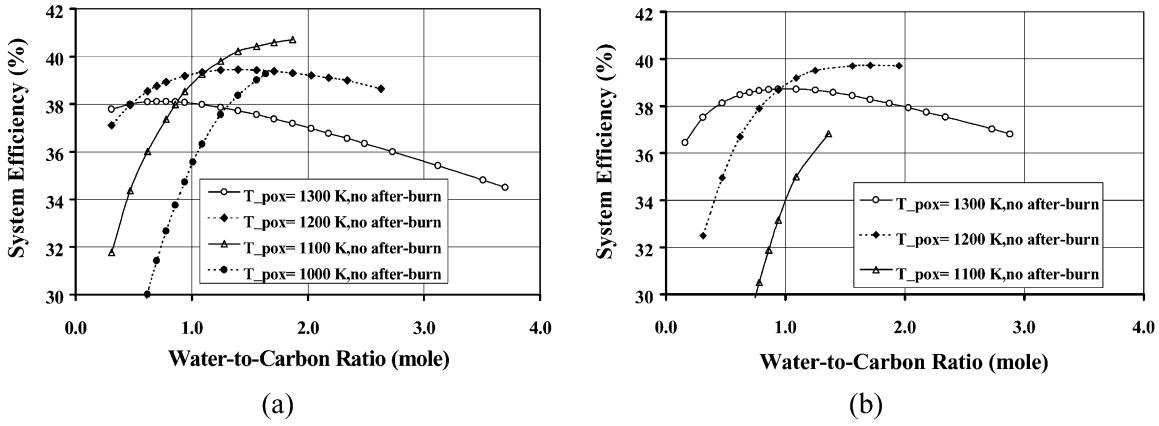

Fig. 17. Total system efficiency without the use of burner heat in the fuel processing subsystem: (a) for the 3 atm system; (b) 1 atm system.

(expander, *gt_1*) for the pressurized system. The net power generated in the system is calculated by subtracting the sum of the parasitic powers consumed by the compressor, fans, and pumps from the total power generated.

For the set of assumptions used in these analyses, Fig. 17 shows η_{SYS} for the cases where the burner heat is not used in the fuel processing subsystem, and Fig. 18 shows the results when the burner heat is used for fuel processing. Without the use of burner heat in fuel processing, Fig. 17 shows that the pressurized system offers somewhat higher η_{SYS} than the atmospheric pressure system for T_{POX} less than 1300 K. Further, the maximum η_{SYS} increases significantly with decreasing T_{POX}. The higher reforming temperatures do, however, permit correspondingly higher amounts of S/C to be used in the fuel processor, which may be required from practical considerations of fuel processor operation.

Using the burner, heat decreases η_{SYS} for the 3 atm system (Fig. 18a versus Fig. 17a) for all reforming temperatures. This is because after heating the process water in *wat_econ2*, less energy is then available for recovery in the expander, *gt_1*. For the 1 atm system, the increase in η_{SYS} is marginal for $T_{POX} = 1300$ K. However, at lower reforming temperatures, for the 1 atm system, the η_{SYS} increases significantly with the use of the burner heat. Indeed, such a 1 atm system operating with a reforming temperature of 1000 K and an S/C approaching 2 showed the highest η_{SYS} (41.9%) of any calculated values for the various parameters examined in this study.

The effect of reducing U_f from 85 to 75% on η_{SYS} is shown in Fig. 19 for the cases without the use of burner heat and in Fig. 20 for the cases with the use of burner heat in the fuel processing subsystem, respectively. In all cases, the lower fuel utilization leads to significantly lower system efficiencies. This might seem surprising at first, since the difference in the fuel processor efficiencies between the two cases of $U_f = 85\%$ and $U_f = 75\%$ is very small (as shown in Fig. 16). The definition of the fuel processor efficiency depends on the amount of hydrogen formed, regardless of the percentage of this amount of hydrogen that is used (fuel utilization) in the fuel cell stack to generate power. To a first order, the amount of fuel needed to operate the fuel cell system is inversely proportional to the fuel utilization used in the fuel cell stack. Therefore, as U_f decreases from 85 to 75%, the amount of fuel needed will increase by the ratio of 85/75 (1.13). Consequently, the system efficiency will decrease by the same ratio of 75/85 (0.88).

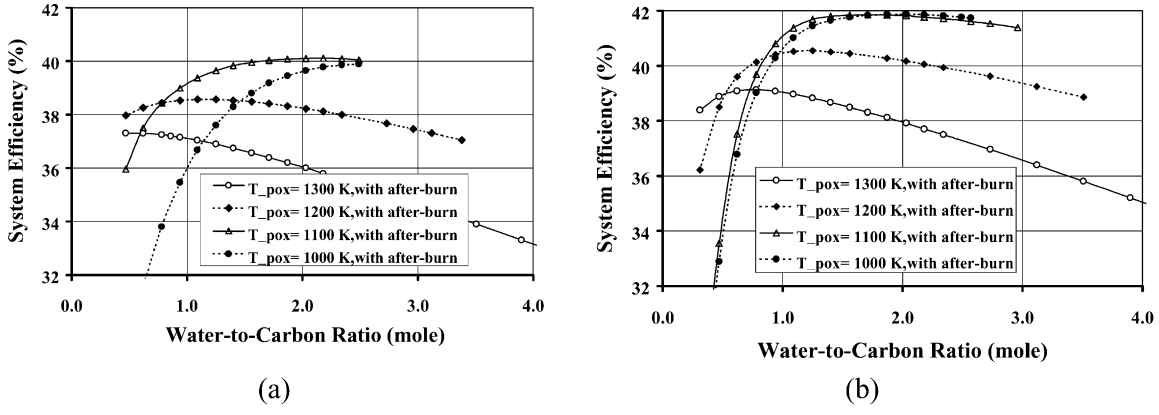

Fig. 18. Effect of using the burner heat for fuel processing on the total system efficiency: (a) in the 3 atm system; (b) 1 atm system.

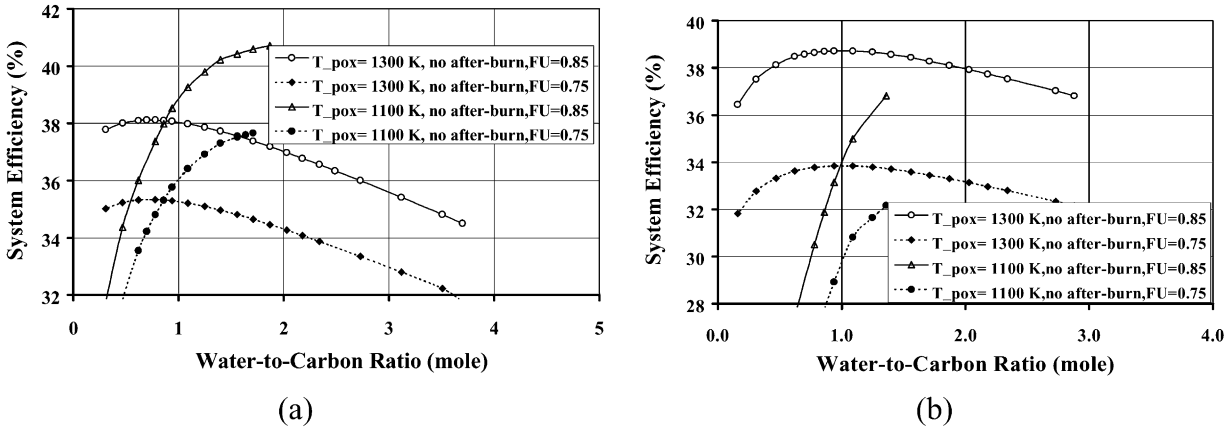

Fig. 19. Influence of electrochemical fuel utilization on total system efficiency without the use of burner heat in the fuel processing subsystem: (a) in the 3 atm system; (b) 1 atm system. Note that the *y*-axis is different in the two subplots.

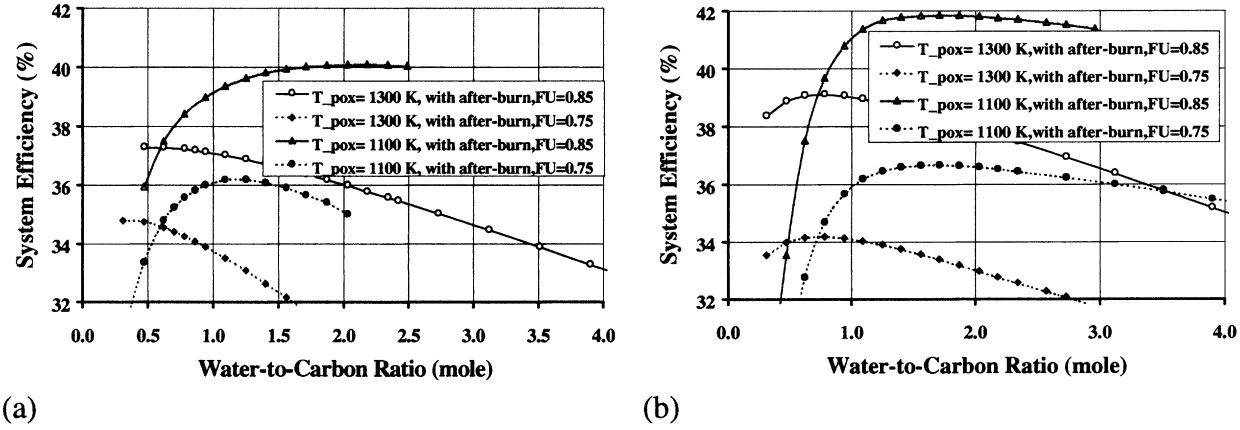

Fig. 20. Effect of using the burner heat in the fuel processing subsystem for two different fuel utilizations: (a) in the 3 atm system; (b) 1 atm system.

6. Summary and conclusions

A parametric study has been performed for an autothermal-reformed gasoline-fueled PEFC system. The analyses were performed to investigate the influence of a variety of design and operating parameters, as well as the degree of thermal integration designed into the fuel processor and the system configuration employed, on the efficiencies of the fuel processor and of the total system. Two major design parameters that were considered in the analysis are the system pressure, nominally 3 and 1 atm, and whether or not thermal energy from the fuel cell exhaust burner is used in the fuel processing subsystem. Other variables examined were the autothermal reforming temperature, T_{POX}, and the electrochemical fuel utilization in the fuel cell stack, U_f. The results were presented as functions of the water-to-carbon mole ratio, S/C, in the feed to the ATR reactor.The results of the parametric study are summarized below.

- The total water-to-carbon that can be used in the fuel processing subsystem is strongly affected by the autothermal reforming temperature. Increasing the reforming temperature increases the amount of water that can be used in the fuel processor (Fig. 4).
- Use of the thermal energy from the fuel cell stack exhaust burner in the fuel processing subsystem permits the use of larger amounts of water in fuel processing. This is due to the increase of the total thermal energy available to heat the process water (Fig. 5).
- Higher reforming temperatures lead to lower fuel equivalence ratios (Figs. 6 and 7), which in turn lead to lower hydrogen concentrations in the reformate.
- Higher reforming temperatures along with the higher amount of water used in the fuel processor lead to lower concentrations of CO at the exit from the low-temperature water–gas shift reactor (Figs. 8 and 9). This decreases the CO removal duty of the preferential oxidation unit.
- Lower reforming temperatures below about 1100 K, lead to the formation of higher concentration of methane in the reformer (Figs. 10 and 11). This in turn leads to decreasing the amount of hydrogen generated for electrochemical oxidation in the fuel cell stack.
- Lower reforming temperatures yield higher fuel processor efficiencies, particularly if the burner heat is used to

increase the amount of water used in fuel processing (Fig. 15). Without the use of burner heat in the atmospheric pressure system, lower reforming temperatures yield substantially lower fuel processor efficiencies (Fig. 14).

- Fuel processor efficiencies are slightly affected by reducing the electrochemical fuel utilization from 85 to 75% in the fuel cell stack (Fig. 16). However, the total system efficiency is reduced significantly by lowering the fuel utilization. This is shown in Figs. 19 and 20, for both the pressurized and atmospheric pressure systems, with and without the use of the burner heat.

As for the two systems considered in this analysis, it is suggested that in order to obtain a high efficiency for the total system, it would be desirable to operate at a reforming temperature of 1000–1100 K, a water-to-carbon mole ratio of 1.5–2.5 at the reformer for both systems, and also to strongly recommend use the burner heat in the fuel processor for the atmospheric system.

It should be emphasized here that the results discussed above are subject to the various assumptions used in the analyses. One such is the assumption of thermodynamic equilibrium at the ATR exit and again at the exit from the water–gas shift reactors (with the methane frozen as at the reformer exit). With these assumptions, the analyses could be carried out to relatively low reforming temperatures and to relatively low values of the water-to-carbon mole ratio in the fuel processor. In practice, however, gasoline contains species that tend to form carbon during the autothermal reforming step. Therefore, significantly higher reforming temperatures and/or water-to-carbon ratios may be required. The higher reforming temperatures may also be needed to provide adequate kinetics for the reforming reactions. As such, the highest fuel processor and system efficiencies presented above may not be achievable.

These analyses do indicate, however, the potential for increased fuel processor and fuel cell system efficiencies if more active catalysts designed can be developed for lower temperature operation. With such catalysts, it might be possible to suppress or reduce methane formation. This could lead to a higher content of hydrogen and a better fuel processor performance. Experimental data with different catalysts are needed to validate the conclusions of the subject analyses.

The results for the overall system performance are also subject to several other assumptions, such as the average cell operating voltage in the fuel cell stack, and the efficiencies of the compressor and expander (for the pressurized system), and of the various pumps, blowers, and fans that are used in the balance-of-plant in the fuel cell system. Changes in those assumptions would affect the actual system efficiency attained, and to a lesser degree the actual fuel processor efficiency. However, the trends identified and discussed above should still be representative of the fuel processor and fuel cell system performance.

All of the results discussed above are for steady-state operation of the fuel cell system at its design rated power level. These analyses did not include part-load or transient operation, some of which has been discussed elsewhere [7–10].

Acknowledgements

This research was sponsored by the US Department of Energy, Office of Advanced Automotive Technologies, Office of Transportation Technologies under Contract W-31-109-ENG-38.

References

[1] J. Mauzey, R. Woods, S. Barge, Automotive fuel processor, in: Proceedings of the 2000 Fuel Cell Seminar Abstracts, Portland, OR, 30 October–2 November 2000, pp. 256–259.
[2] A. Heinzel, B. Vogel, T. Rampe, A. Haist, P. Hubner, Reforming of fossil fuels — R&D Fraunhofer institute for solar energy systems, in: Proceedings of the 2000 Fuel Cell Seminar Abstracts, Portland, OR, 30 October–2 November 2000, pp. 260–262.
[3] W.L. Mitchell, M. Hagen, S.K. Prabu, Gasoline Fuel Cell Power Systems for Transportation Applications: A Bridge to the Future of Energy, SAE Paper no. 1999-01-0535, Society of Automotive Engineers, 1999.
[4] T. Flyn, Multifuel processor for fuel cell electric vehicles applications, The 2000 Annual Progress Report on Transportation Fuel Cell Power System, DOE Office of Transportation Technologies, US, October 2000.
[5] S. Ahmed, S.H. Lee, E. Doss, C. Pereira, D. Colombo, M. Krumpelt, Integrated fuel processor development, The 2000 Annual Progress Report on Transportation Fuel Cell Power System, DOE Office of Transportation Technologies, US, October 2000.
[6] H.K. Geyer, R.K. Ahluwalia, GCtool for Fuel Cell System Design and Analysis: User Documentation, Argonne National Laboratory Report ANL-1998/8, Argonne, IL, March 1998.
[7] R. Kumar, E.D. Doss, R. Ahluwalia, H. Geyer, Performance requirements for a gasoline-fueled automotive fuel cell system to meet the PNGV target of 80 miles per gallon, in: Proceedings of the 2000 Fuel Cell Seminar Abstracts, Portland, OR, 30 October–2 November 2000, pp. 272–275.
[8] E.D. Doss, R.K. Ahluwalia, R. Kumar, Pressurized and atmospheric pressure gasoline-fueled polymer electrolyte fuel cell system performance, in: Proceedings of the 34th Intersociety Engineering Conference on Energy Conversion (IECEC), SAE Technical Paper 1999-01-2574, Vancouver, BC, 2–5 August 1999.
[9] R. Kumar, R. Ahluwalia, E.D. Doss, H.K. Geyer, M. Krumpelt, Design integration and trade-off analyses of gasoline-fueled polymer electrolyte fuel cell systems for transportation, in: Proceedings of the 1999 Fuel Cell Seminar, Palm Springs, CA, 16–19 November 1998, pp. 226–229.
[10] E.D. Doss, R.K. Ahluwalia, R. Kumar, Analytical performance of direct hydrogen-fueled polymer electrolyte fuel cell systems for transportation applications, in: Proceedings of the 33th Intersociety Engineering Conference on Energy Conversion (IECEC), Colorado Springs, CO, 2–6 August 1998.